Mechanical signalling via membrane tension drives saltatory neuronal migration

Takunori Minegishi[1,*], Honami Hasebe[1], Tomoya Aoyama[2], Keiji Naruse[3] Yasufumi Takahashi[2,4] and Naoyuki Inagaki[1,*]

[1]Laboratory of Systems Neurobiology and Medicine, Division of Biological Science, Nara Institute of Science and Technology, Nara 630-0192, Japan

[2]WPI Nano Life Science Institute, Kanazawa University, Kanazawa, Ishikawa 920-1192, Japan

[3]Department of Cardiovascular Physiology, Graduate School of Medicine, Dentistry and Pharmaceutical Sciences, Okayama University, Okayama 700-8558, Japan

[4]Department of Electrical Engineering, Graduate School of Engineering, Nagoya University, Nagoya, Aichi 464-8601, Japan

[*]Corresponding authors: Takunori Minegishi; E-mail: t-minegishi@bs.naist.jp. Naoyuki Inagaki; E-mail: ninagaki@bs.naist.jp.

Abstract

Neurons migrate through repeated leading process extension and somal translocation, yet how they coordinate these movements remains unknown. Here, we demonstrate that leading process extension increases plasma membrane tension and triggers Ca^{2+} influx via mechanosensitive ion channels, leading to actomyosin contraction for somal translocation. Thus, membrane tension transduces the change in the leading process length into a force that drives somal translocation, allowing saltatory and efficient movement of neuronal migration.

Neuronal migration is essential for brain development and neural network formation[1-3]. As a characteristic feature of their migration, neurons navigate in a saltatory manner by repeating two steps[2, 4]. Navigation is initiated by the extension of the leading process, which determines the migratory route in response to extracellular guidance cues[5]. This is followed by somal translocation. Since the soma is the largest part of the cell, its translocation relies on the generation of robust forces to overcome mechanical barriers in the surrounding environment[6, 7]. A previous study reported that leading process extension of olfactory interneurons is triggered by shootin1b accumulation at the growth cone, which generates the traction force required for extension[8]. On the other hand, Ca^{2+} signalling induces actomyosin contraction at the cell rear, thereby producing a force to propel somal translocation[7, 9]. Efficient and saltatory neuronal migration requires coordination between the leading process extension and somal translocation; however, the signalling pathway that couples these two steps remains unexplored. Here, we show that the leading process extension of migrating neurons increases their plasma membrane tension. This tension elevation activates the mechanosensitive ion channel Tmem63b and triggers Ca^{2+} signalling, activating actomyosin at the rear of the cell. Blockade of this tension-mediated signalling by Tmem63b knockdown disturbs neuronal saltatory movement and inhibits neuronal migration, demonstrating its involvement in efficient saltatory neuronal migration.

Results

Leading process extension increases plasma membrane tension

To identify the signalling events triggered by leading process extension, we first analysed the plasma membrane tension. Lamoureux et al. reported that axonal extension of chick

sensory neurons increased neurite tension[10], suggesting that plasma membrane tension may also increase in a neurite length-dependent manner. To examine this possibility, we analysed the membrane tension of migrating mouse olfactory interneurons by measuring the fluorescence lifetime of the membrane tension-sensitive probe Flipper-TR[11]; a longer fluorescence lifetime of the probe indicates higher membrane tension. Fig. 1a shows the spatial distribution of the membrane tension, which was higher at the leading process growth cone (arrowheads, Fig. 1a, b). Analyses of neurons bearing leading processes of different lengths demonstrated a significant positive correlation between the process length and membrane tension in the soma and leading process shaft (Fig. 1a, c).

To examine whether the leading process extension increases the membrane tension, we performed time-lapse imaging. As repetitive imaging of Flipper-TR damaged neurons, we analysed the tension with scanning ion conductance microscopy (SICM)[12], which has been used to monitor membrane tension through cell stiffness measurements (see Materials and Methods)[12, 13]. Consistent with the above data, the stiffness was higher at the growth cone (arrowhead, Fig. 1d) and uniform across the leading process shaft and soma. The membrane stiffness in a proximal region of the leading process was increased by extension of the process and decreased by its shortening (Fig. 1e). Moreover, the increased stiffness was significantly positively correlated with the increase in the leading process length (Fig. 1f). Overall, these data indicate that the extension of the leading process increases the plasma membrane tension.

Increased membrane tension due to leading process extension triggers Ca^{2+} signalling

Previous studies reported that increases in the plasma membrane tension propagate rapidly and triggers cell signalling through mechanosensitive ion channels[14-18]. We next investigated the relationship between leading process extension and Ca^{2+} signalling. The intracellular Ca^{2+} concentration ($[Ca^{2+}]_i$) of olfactory interneurons was monitored using the Ca^{2+} indicator CalRedR525/650 (Fig. 2a and Supplementary Video 1). The average neurite length was 39.0 ± 2.7 μm (mean ± SEM, n =14 cells) and the neurites extended and retracted 11.3 ± 0.7 μm (29.0 ± 1.8% of the neurite length). Remarkably, the frequency of the Ca^{2+} transients increased when the leading process length was 4 μm larger than the average length (Fig. 2b, c).

Leading process extension is driven by the traction force of the leading process growth cone[8]. We previously reported that shootin1b mediates the production of the traction force at the growth cone[8] (Extended Data Fig. 1a). Importantly, the reduction in the process length by shootin1 knockout (KO) decreased the frequency of Ca^{2+} transients (Extended Data Fig. 1b-d and Supplementary Video 2). We also increased the leading process length using a cell-stretching device (Extended Data Fig. 2); increasing the process length by 20% increased the frequency of Ca^{2+} transients (Fig. 2d, f and Supplementary Video 3). On the other hand, no effect was observed when the stretch was applied perpendicular to the leading process (Fig. 2e, f). Furthermore, treatment of neurons with 5 μM GsMTx4, which inhibits mechanosensitive ion channels[19], reduced the frequency of Ca^{2+} transients (Fig. 2g and Extended Data Fig. 3). Thus, we conclude that the increased membrane tension caused by the leading process extension triggers Ca^{2+} signalling through mechanosensitive ion channels.

Tmem63b mediates tension-triggered Ca^{2+} signalling

To identify the molecule involved in the tension-mediated Ca^{2+} signalling process, we analysed the expression of mechanosensitive ion channels through quantitative PCR (qPCR) and found that Tmem63b is highly expressed in olfactory interneurons (Fig. 2h). Repression of Tmem63b by miRNA suppressed spontaneous Ca^{2+} transients (Fig. 2i, red and Extended Data Fig. 4a-c) and abolished tension-triggered Ca^{2+} transients (Fig. 2i, blue). Furthermore, expression of RNAi-refractory Tmem63b rescued the inhibition of spontaneous and tension-triggered Ca^{2+} transients (Fig. 2i and Extended Data Fig. 4d), indicating that Tmem63b is involved in tension-triggered Ca^{2+} signalling by olfactory interneurons.

Tension-triggered Ca^{2+} signalling drives somal translocation

Ca^{2+} signalling activates the myosin light chain kinase-myosin II pathway[20]. Therefore, we examined whether the activation of Tmem63b triggers actomyosin contraction and somal translocation. Immunostaining analyses of phosphorylated myosin light chain (pMLC) showed that stretching of the leading process elevated myosin II activity at the rear of the cell (Fig. 3a, b and Extended Data Fig. 5). Furthermore, this activation was abolished by Tmem63b knockdown (Fig. 3a, b). When Tmem63b was knocked down, neurons extended a long leading process; however, the soma did not translocate efficiently in response to the process extension (Fig. 3c, d and Supplementary Video 4). Moreover, neurons showed reduced somal translocation speeds (Fig. 3e) and impaired saltatory movement (Fig. 3c, d and Supplementary Video 4). Importantly, the disturbance in the saltatory movement was accompanied by a significant reduction in the neuronal migration speed (Fig. 3f). Similar inhibition was observed in neurons treated with the MLC kinase inhibitor ML-7 (10 μM) or the myosin II inhibitor blebbistatin (100 μM)

(Extended Data Fig. 6). Furthermore, expression of RNAi-refractory Tmem63b in neurons expressing Tmem63b miRNA rescued extension-triggered myosin II activation as well as the saltatory movement and migration speed (Fig. 3a-f, Supplementary Video 4). Taken together, these data indicate that tension-triggered Ca^{2+} signalling drives somal translocation through myosin II activation.

Discussion

In this study, we showed that leading process extension of migrating neurons increases membrane tension. This tension elevation activates the mechanosensitive ion channel Tmem63b and triggers Ca^{2+} signalling, which drives somal translocation through actomyosin contraction. Our work presents an integrated model of saltatory neuronal migration (Fig. 3g) involving a series of biochemical (magenta) and mechanical (blue) steps, providing a missing link to supplement previous findings. (i) Shootin1b accumulation at the growth cone generates the traction force and triggers leading process extension (Extended Data Fig. 1a)[8]. (ii) The leading process extension increases the membrane tension, which activates Tmem63b and triggers Ca^{2+} signalling. (iii) Upon activation by Ca^{2+} signalling, actomyosin produces contractile forces, pushing the nucleus forwards and driving somal translocation[7, 9]. This is followed by shootin1b accumulation at the growth cone, initiating the next cycle.

We speculate that dysregulation of the signalling pathway through membrane tension may occur in diseases caused by neuronal migration defects, including brain malformation, intellectual disability and epilepsy[2, 3, 21, 22]. After migration, neurons undergo dynamic morphological changes to perform their activities, including, polarity formation, axon guidance, synapse formation, synaptic plasticity, transmitter release and

neural network regeneration. Similar mechanical processes might regulate these activities as they may also change the plasma membrane tension.

Materials and Methods

Animals

All relevant aspects of the experimental procedures were approved by the Institutional Animal Care and Use Committee of Nara Institute of Science and Technology. Postnatal day 5 (P5) C57BL/6 mice were obtained from Japan SLC and CLEA Japan. P5 Shootin1 KO pups were obtained by crossing male and female shootin1 heterozygous mice; the offspring genotypes were checked by PCR with the following primers: Genotyping F1 (5′-CAGACTGCTACCCACTACCCCCTAC-3′) and Genotyping R1 (5′-CCTAGAGCTGGACAGCGGATCTGAG-3′) for the WT allele; Genotyping F2 (5′-CCCAGAAAGCGAAGGAACAAAGCTG-3′) and Genotyping R2 (5′-ACCTTGCTCCTTCAAGCTGGTGATG-3′) for the shootin1 KO allele. Shootin1 KO pups and their littermates were bred with their mother under standard conditions (12 h/12 h light/dark cycle, access to dry food and water). Mice of both sexes were used for experiments. The generation of shootin1 KO mice is described elsewhere[23]. Chimeric mice were crossed with C57BL/6 mice for at least nine generations before analysis.

DNA construction

To generate a Tmem63b miRNA expressing vector, we used a Block-iT Pol II miR RNAi expression vector kit (Thermo Fisher Scientific). The targeting sequence of Tmem63b (5′-CGAGGACAGCCTCATAGAGAA-3′, corresponding to nucleotides 2424-2444 in the coding region of mouse Tmem63b) was cloned and inserted into the pcDNA6.2-GW/EmGFP-miR expression vector. To prevent signal overlap between the GFP reporter of the miRNA expression vector and the fluorescent dyes used in our experiments, a DNA cassette containing the miRNA sequence was subcloned and inserted into pEBFP-C1 (Takara Bio) and pmCherry-C1 (Takara Bio) for Ca^{2+} imaging and immunocytochemical analyses, respectively. Full-length cDNA of mouse Tmem63b was obtained by PCR amplification of mouse subventricular zone (SVZ) cDNA with the primers Tmem63b Fw (5′-GACGACGATGACAAGAGATCTATGCTGCCGTTCTTGCTGGCCACA-3′) and Tmem63b Rv (5′-GATACGCGTGGTACCAGATCTTTACTGGTGAATCTCATTCTCTAT-3′), and subcloned and inserted into pCMV5-FLAG vector (Agilent Technology). The mouse SVZ cDNA was prepared as described in the ‘qPCR analysis of migrating neurons’

section. The RNAi refractory Tmem63b mutant was generated by inducing seven silent mutations in nucleotides 2424-2444 of Tmem63b (5′-TGAAGATAGTCTGATTGAAAA-3′; the underlines indicate the mutations) by PCR.

Culture of dissociated SVZ-derived olfactory interneurons and transfection

SVZ tissues dissected from P5 mouse brains were dissociated with papain (Nacalai Tesque) as previously described[8]. The dissociated olfactory interneurons were reaggregated in neurobasal medium (Thermo Fisher Scientific) containing 10% fetal bovine serum (Thermo Fisher Scientific), 2% B-27 supplement (Thermo Fisher Scientific), 1 mM glutamine (Nacalai Tesque) and 100 U/mL penicillin–streptomycin (Nacalai Tesque) for 5-7 h. The aggregates were then embedded in a mixture of 75% Matrigel (Corning) and 25% Leibovitz′s L-15 (L-15) medium (Thermo Fisher Scientific), plated on glass bottom dishes (Matsunami) or elastic silicon chambers (Strex, catalogue number STB-CH-04), and cultured in neurobasal medium containing 2% B-27 supplement, 1 mM glutamine and 100 U/mL penicillin–streptomycin in a humidified 5% CO_2 incubator at 37°C. For cell stiffness measurements by SICM, the dissociated olfactory interneurons were cultured on glass bottom dishes coated subsequently with 100 μg/mL poly-D-lysine (Sigma) and 5 μg/mL laminin (Wako Pure Chemical Industries) as previously described[8]. For RNAi experiments, olfactory interneurons were transfected with vectors using Nucleofector (Lonza) before reaggregation. For the immunoblot analysis shown in Extended Data Fig. 4a, transfected olfactory interneurons were cultured on poly-D-lysine-coated plastic dishes.

Analysis of plasma membrane tension by Flipper-TR

After 2 days of culture in Matrigel, olfactory interneurons were incubated with 1 μM of the membrane tension-sensitive probe Flipper-TR (Spirochrome) diluted in culture medium for 1 h at 37°C and 5% CO_2. Then the culture medium was replaced with L-15 medium containing 2% B-27 supplement, 1 mM glutamine and 100 U/mL penicillin–streptomycin. Fluorescence lifetime imaging microscopy (FLIM) analysis was performed at 37°C using a confocal laser scanning microscope (SP8, Leica) equipped with a Fast Lifetime Contrast (FALCON) module, HC PL APO CS2 100x/1.40 oil immersion lens, and imaging software Las-X (Leica). The cells were excited with a pulsed 488 nm laser operating at 80 MHz, and the emission signals were detected at 575-625 nm. Following imaging, a double exponential fitting was performed to ensure a close fit (chi squared <

1.5). For quantification, we manually identified a plasma membrane region and measured the average lifetime within this region.

Time-lapse imaging of plasma membrane tension by SICM

As an increase in the plasma membrane tension leads to decreased membrane deformability[24], membrane stiffness has been used as an indicator of plasma membrane tension. SICM can be used to measure membrane stiffness without directly contacting the membrane and has been used to estimate membrane tension[12, 13]. In SICM, a glass nanopipette is used as a probe to monitor ion currents between an Ag/AgCl electrode placed inside the pipette and an Ag/AgCl electrode located in a bath. A constant pressure is applied to the pipette to generate a microfluidic flow, which deforms the cell surface. As the pipette approaches the cell, the ion current decreases. This decrease is slower for softer cells because the microfluidic flow progressively indents the cell surface. Therefore, the plasma membrane stiffness can be determined based on the ion current approach curve[12].

The plasma membrane tension was measured using a homemade SICM system with an inverted optical microscope (Eclipse-Ti, Nikon). The setup of the SICM system, the scanning algorithms and the protocol were described previously[25]. Before the measurements were acquired, the culture medium was replaced with L-15 medium containing 2% B-27 supplement, 1 mM glutamine and 100 U/mL penicillin–streptomycin. Glass nanopipettes (aperture inner radius 100 nm) filled with L-15 medium were used as probes. Scanning was performed in hopping mode with the following parameters: hopping amplitude, 3-5 μm; waiting time after lateral movement, 1 ms (during this time, a reference current was measured as the average of the direct current through the probe); probe approach and withdrawal speed, 20 and 500-1000 nm/ms, respectively; applied pressure, 10 kPa; and set point, 98% of the reference current. We recorded ion currents and the vertical probe position as the probe approach the cell surface. For the experiments shown in Fig. 1d, we obtained data for a 25 x 25 μm^2 area containing 128 x 128 points. For the experiments shown in Fig. 1e and 1f, we obtained data for a 10 x 10 μm^2 area containing 32 x 32 points, and repeated the experiment 3 times for each cell at 1 h intervals. After the measurements were performed, optical cell images were acquired using a CSI S Plan Fluor ELWD 40x/0.6 NA objective lens (Nikon), a complementary metal oxide

semiconductor (CMOS) camera (ORCA Flash 4.0 C13440-20CU, Hamamatsu) and imaging software (HCI image, Hamamatsu) or using a Plan Flour 10x/0.30 NA objective lens (Nikon), a CMOS camera (Wraycam-noa2000, Wraymer) and imaging software (MicroStudio, Wraymer). The SICM data were analysed and stiffness maps were produced using a handmade program developed based on LabVIEW2014 (National Instruments). The approach curve of each point was plotted as the ion current versus the vertical probe position, and the slope between 98.5% and 99% of the reference current was determined with a line fit. Young's modulus of the cell surface was determined as described previously[12]:

$$E = p_0 A \left(\frac{s_\infty}{s} - 1\right)^{-1}$$

where E is Young's modulus, p_0 is the applied pressure, A is the pipette geometrical parameter (whose value is 0.4, as determined previously[12]), and s and s_∞ are the measured slopes on the cell surface and substrate, respectively.

Ca^{2+} imaging

$[Ca^{2+}]_i$ was monitored using the ratiometric calcium indicator dye CalRed R525/650 AM (AAT Bioquest); when this indicator is excited at 488 nm upon Ca^{2+} binding, the emission signals increased at 525 nm and decreased at 650 nm. After 2 days in culture, olfactory interneurons were loaded with 1 μM CalRed R525/650 AM, 0.1% DMSO (Sigma) and 0.04% F-127 (AAT Bioquest) diluted in the culture medium for 1 h at 37°C and 5% CO_2. The cells were subsequently washed with the culture medium. Before imaging, the culture medium was replaced with prewarmed artificial cerebrospinal fluid (ACSF) (10 mM HEPES, pH 7.4, 125 mM NaCl, 25 mM glucose, 2.5 mM KCl, 2 mM $CaCl_2$, 1 mM $MgCl_2$). Imaging was performed at 37°C using a confocal microscope (LSM710, Carl Zeiss) equipped with a Plan-Apochromat 20x/0.8 objective lens. The dye-loaded olfactory interneurons were excited with a 488 nm argon laser, and the emission signals were detected simultaneously at 525 ± 25 nm and > 611 nm. Differential interference contrast (DIC) and fluorescence images were acquired at 5 sec intervals for 15 min or 30 min. To image cells expressing miRNA, EBFP fluorescence was used as an indicator of transfected cells. $[Ca^{2+}]_i$ analyses were performed using ImageJ software (NIH). The

fluorescence intensities at 525 nm and 650 nm in the same region were measured over time at the soma. $[Ca^{2+}]_i$ was calculated as the ratio of the fluorescence intensity at 525 nm to the fluorescence intensity at 650 nm. The average of $[Ca^{2+}]_i$ was set as the baseline (F_0), and the $[Ca^{2+}]_i$ in each frame (F) was normalized to the baseline (F/F_0). A change in $[Ca^{2+}]_i$ was judged as a Ca^{2+} transient if $F/F_0 > 40\%$.

Mechanical stretching of the leading process

Neurons suspended in a mixture of 75% Matrigel and 25% L-15 medium were plated on elastic chambers and cultured for 2 days as described above. For Ca^{2+} imaging, after a control image was acquired, the chamber was set on the stretching device (Strex, catalogue number STB-CH-04ST-20) and stretched uniaxially (20% stretch, Extended Data Fig. 2a). We then identified the same cell and acquired Ca^{2+} images after the stretching process. We also measured the angle of the leading process with respect to the stretch direction (θ) (Extended Data Fig. 2b). When the angle was between 0° and 30°, we determined that the leading process was extended (parallel extension). On the other hand, when the angle was between 60° and 90°, the stretch direction was determined to be perpendicular to the leading process. For immunocytochemical analysis, olfactory interneurons were subjected to 20% uniaxial stretch for 15 min at 37°C before fixation.

Analyses of neuronal migration in Matrigel

Before observation, the culture medium was replaced with L-15 medium containing 2% B-27 supplement, 1 mM glutamine and 100 U/mL penicillin–streptomycin. Phase contrast images were acquired every 2 min for 2 h at 37°C using a fluorescence microscope (IX81, Olympus) equipped with Plan Fluar 40x, 0.60 NA (Olympus) and an electron multiplying-CCD camera (EMCCD, iXon DU888, Andor) and MetaMorph. To image the cells expressing miRNA, mCherry fluorescence was used as an indicator of transfected cells. Time-lapse images were analysed and quantified using ImageJ and the manual tracking plugin. The migration speed (Fig. 3f) was calculated by dividing the migration distance of the soma by the observation time. When the soma translocated any distance during the 2-min image acquisition intervals, we judged that neurons were in the somal translocation phase. The somal translocation speed (Fig. 3e) was calculated by dividing the migration distance of the soma during the somal translocation phase by the

observation time.

qPCR analysis of migrating neurons

SVZ explants were prepared and cultured as previously described[8]. Briefly, the SVZs were dissected from the P5 mouse brains and cut into blocks 100-150 μm in diameter. The SVZ tissue blocks were then embedded in a mixture of 75% Matrigel and 25% L-15 medium, and cultured in neurobasal medium containing 2% B-27 supplement, and 1 mM glutamine in a humidified 5% CO_2 incubator at 37°C. After 2 days in culture, the SVZ blocks were removed from the olfactory interneurons that migrated out from the blocks. Then, the total RNA of the migrating neurons was isolated using an RNeasy mini kit (Qiagen) according to the manufacturer′s protocol followed by DNaseI digestion (Thermo Fisher Scientific, catalogue number 11766051). The RNA was then reverse transcribed into cDNA using Superscript IV VILO master mix (Thermo Fisher Scientific) according to the manufacturer′s protocol, and cDNA was used in the qPCR assays. qPCR assays were performed using the LightCycler 96 system (Roche), KAPA SYBR FAST qPCR kit (Nippon Genetics) and the following primer sets: Piezo1, 5′-TTGACCCTGCCAACTGGTTT-3′ and 5′-GCCTCAAACACCAGCAACAG-3′; Piezo2, 5′-GTATTGGATCTACGTCTGCGG-3′ and 5′-CAGGATCTTCCTCCACCACTCG-3′; TRPC1, 5′-CAGAAGGACTGTGTGGGCAT-3′ and 5′-GAACAGAGCAAAGCAGGTGC-3′; TRPC3, 5′-AGTGTCTGGTCGTGTTGGTC-3′ and 5′-AAGAATCTTCCCCAGCCTGC-3′; TRPC5, 5′-TACCAATGTGAAGGCCCGAC-3′ and 5′-TATCAGCATGATCGGCAATG-3′; TRPC6, 5′-GCCGTCCAAATCTCAGCCGTT-3′ and 5′-TGGACAGGAGCTGTTGCTGAC-3′; TRPV2, 5′-GTTTGACCGTGACCGACTCT-3′ and 5′-CGTCTTTCCAGTGGAGCCTT-3′; TRPV4, 5′-GCTTCTTCCAGCCCAAGGAT-3′ and 5′-TGTCGCCTCATGTCAGCTTT-3′; TRPA1, 5′-ACAAGAAAGCCAGCCCTCTC-3′ and 5′-GGTTGCAGCAAAATGGAGGG-3′; TACAN, 5′-CTGCAGCAGGACTTCCAAGGT-3′ and 5′-CAGTTGGCCTGGAGTTTGGTC-3′; Tmem63a, 5′-CAGGGCAACAAGACTTTGAA-3′ and 5′-TGTGCCTCTGAAAAGACAGG-3′; Tmem63b, 5′-AGAACAGGACGACCATGCACA-3′ and 5′-

AGAGCCAGCGGAAGAAGAGGT-3′; GAPDH, 5′-TGATGGGTGTGAACCACGAG-3′ and 5′-GGCATGGACTGTGGTCATGA-3′.

Preparation of cell lysate and immunoblotting

Cultured neurons were lysed with RIPA buffer (50 mM Tris-HCl (pH 8.0), 1 mM EDTA, 150 mM NaCl, 1% Triton X-100, 0.1% SDS, 0.1% sodium deoxycholate, 1 mM DTT, 1 mM PMSF, and 0.01 mM leupeptin), and incubated for 2 h at 4°C. The cell lysate was then centrifuged at 17900 x *g* for 10 min at 4°C. The supernatant was mixed with an equal volume of 2 x SDS sample buffer (131 mM Tris-HCl, pH 6.8, 21% glycerol, 4% SDS, 0.05% bromophenol blue and 5% β-mercaptoethanol). The mixture was incubated for 2 h at 37°C, followed by SDS-polyacrylamide gel electrophoresis. Immunoblotting was performed as previously described[8]. The following primary antibodies were used in immunoblotting: rabbit anti-Tmem63b (1:200) (Novus Biologicals, catalogue number NBP2-58473), mouse anti-actin (1:10000) (Millipore, catalogue number MAB1501R). The following secondary antibodies were used for immunoblotting: HRP-conjugated donkey anti-rabbit IgG (1:2000) (GE Healthcare, catalogue number NA934) and HRP-conjugated donkey anti-mouse IgG (1:5000) (Bio-Rad, catalogue number 1706516).

Immunocytochemical analysis

Olfactory interneurons subjected to 20% uniaxial stretch were fixed with 4% paraformaldehyde dissolved in Krebs buffer (118 mM NaCl, 4.7 mM KCl, 1.2 mM KH_2PO_4, 1.2 mM $MgSO_4$, 4.2 mM $NaHCO_3$, 2 mM $CaCl_2$, 10 mM glucose, 400 mM sucrose, and 10 mM HEPES (pH 7.0)) for 10 min on ice, followed by treatment with 0.1% Triton X-100 in phosphate-buffered saline (PBS) for 15 min on ice and 10% fetal bovine serum in PBS for 1 h at room temperature. They were then incubated with primary antibody diluted in PBS containing 10% fetal bovine serum overnight at 4°C. The following primary antibodies were used: rabbit anti-myosin light chain 2 (1:500) (Abcam, catalogue number ab79935) and mouse anti-phospho-myosin light chain 2 (Ser19) (1:500) (Cell Signaling Technology, catalogue number 3675). Cells were washed with PBS, and then incubated with secondary antibody and 1 μg/mL DAPI (Thermo Fisher Scientific) diluted in PBS for 1 h at room temperature. The following secondary antibodies were used: Alexa Fluor 647-conjugated donkey anti-rabbit IgG (1:1,000)

(Abcam, catalogue number ab150075) and Alexa Fluor 488 conjugated goat anti-mouse (1:1,000) (Thermo Fisher Scientific, catalogue number A-11029). The immunostained cells were mounted with 50% (v/v) glycerol (Nacalai Tesque) in PBS. Fluorescence images were acquired using a confocal laser microscope (Stellaris 8, Leica) equipped with an HC Plan-Apochromat 20x, 0.75 NA objective lens (Leica) and imaging software (LAS X, Leica). To acquire images of the entire olfactory interneurons, we obtained 6-15 confocal images at 2 μm intervals in the Z axis direction. Then, the confocal images were volume-stacked, and the fluorescence signals were quantified using ImageJ.

Chemicals

The following reagents were used at the indicated concentrations in this study: 5 μM GsMTx4 (Tocris Bioscience), 100 μM blebbistatin (Sigma) and 10 μM ML7 (Tocris Bioscience). A stock solution of GsMTx4 was prepared in H_2O. Stock solutions of blebbistatin and ML7 were prepared in DMSO.

Statistical analysis

Statistical analyses were performed using Excel 2016 (Microsoft) or GraphPad Prism 7 (GraphPad Software). For samples with more than 7 data points, the D′Agostino–Pearson normality test was used to determine whether the data followed a normal distribution. For cases in which the number of data points was between 3 and 7, the Shapiro–Wilk test was used for the normality test. We also tested the equality of variation with the F test for two independent groups that followed normal distributions. Significance tests were performed as follows: (1) two-tailed paired *t*-test to compare normally distributed data from two dependent groups; (2) two-tailed Wilcoxon signed-rank test to compare nonnormally distributed data from two dependent groups; (3) two-tailed unpaired Student′s *t*-test to compare normally distributed data with equal variance from two independent groups; (4) two-tailed unpaired Welch′s *t*-test to compare normally distributed data with unequal variance from two independent groups; (5) two-tailed Mann–Whitney *U*-test to compare nonnormally distributed data from two independent groups; (6) two-tailed one-way ANOVA with Tukey′s post hoc test to compare normally distributed data from three groups; (7) two-tailed Kruskal–Wallis tests with Dunn′s multiple comparison test to

compare nonnormally distributed data from three groups; and (8) two-tailed Spearman's correlation coefficient test to analyse nonnormally distributed data. The statistical information and number of samples for each experiment are indicated in the figure legends. All data are shown as the mean ± SEM. Statistical significance was defined as ***$p < 0.01$; **$p < 0.02$; *$p < 0.05$; ns, not significant. For the experiments using shootin1 KO mice, littermates were allocated into the experimental groups by genotyping. For the other experiments, sample allocation was randomized as cells were derived from the same resource. The numbers for the groups of each sample were based on those in previously published studies. No data were excluded if the experiments were successfully performed. All experiments were performed at least three times and reliably reproduced. Investigators were blind to the experimental groups for each analysis, except biochemical analyses.

Data availability

Data will be made available upon reasonable request.

Code availability

The code used to analyse the SICM data and generate the stiffness maps will be made available upon reasonable request.

Acknowledgements

We thank Dr. Motohiro Nishida for valuable discussions; Mieko Ueda and Kazumi Maekawa for technical support; and Satoko Shimamura for kind encouragement.

Author contributions

T.M., H.H. and T.A. performed the experiments and data analysis. T.M., H.H., T.A., K.N., Y.T. and N.I. designed the experiments. T.M. and N.I. wrote the manuscript. All authors discussed the results and commented on the manuscript.

Funding

This research was supported in part by AMED under Grant Number 22gm0810011h0006 (N.I.), JSPS KAKENHI (JP19H03223, N.I.), JSPS Grants-in-Aid for Early-Career Scientists (JP19K16258 and JP23K14181, T.M.), and the Osaka Medical Research Foundation for Incurable Diseases (T.M.).

Competing interests

The authors declare that they have no competing interests.

References

1. Hatten, M.E. New directions in neuronal migration. *Science* **297**, 1660-1663 (2002).
2. Evsyukova, I., Plestant, C. & Anton, E.S. Integrative mechanisms of oriented neuronal migration in the developing brain. *Annu Rev Cell Dev Biol* **29**, 299-353 (2013).
3. Nakajima, C., Sawada, M. & Sawamoto, K. Postnatal neuronal migration in health and disease. *Curr Opin Neurobiol* **66**, 1-9 (2021).
4. Cooper, J.A. Cell biology in neuroscience: mechanisms of cell migration in the nervous system. *J Cell Biol* **202**, 725-734 (2013).
5. Marin, O., Valiente, M., Ge, X. & Tsai, L.H. Guiding neuronal cell migrations. *Cold Spring Harb Perspect Biol* **2**, a001834 (2010).
6. Solecki, D.J. *et al.* Myosin II motors and F-actin dynamics drive the coordinated movement of the centrosome and soma during CNS glial-guided neuronal migration. *Neuron* **63**, 63-80 (2009).
7. Martini, F.J. & Valdeolmillos, M. Actomyosin contraction at the cell rear drives nuclear translocation in migrating cortical interneurons. *J Neurosci* **30**, 8660-8670 (2010).
8. Minegishi, T. *et al*. Shootin1b mediates a mechanical clutch to produce force for neuronal migration. *Cell Rep* **25**, 624-639 e626 (2018).

9. Komuro, H. & Rakic, P. Intracellular Ca2+ fluctuations modulate the rate of neuronal migration. *Neuron* **17**, 275-285 (1996).

10. Lamoureux, P., Buxbaum, R.E. & Heidemann, S.R. Direct evidence that growth cones pull. *Nature* **340**, 159-162 (1989).

11. Colom, A. *et al.* A fluorescent membrane tension probe. *Nat Chem* **10**, 1118-1125 (2018).

12. Rheinlaender, J. & Schaffer, T.E. Mapping the mechanical stiffness of live cells with the scanning ion conductance microscope. *Soft Matter* **9**, 3230-3236 (2013).

13. Bednarska, J. *et al.* Rapid formation of human immunodeficiency virus-like particles. *Proc Natl Acad Sci U S A* **117**, 21637-21646 (2020).

14. Lee, J., Ishihara, A., Oxford, G., Johnson, B. & Jacobson, K. Regulation of cell movement is mediated by stretch-activated calcium channels. *Nature* **400**, 382-386 (1999).

15. Houk, A.R. *et al.* Membrane tension maintains cell polarity by confining signals to the leading edge during neutrophil migration. *Cell* **148**, 175-188 (2012).

16. Tsujita, K., Takenawa, T. & Itoh, T. Feedback regulation between plasma membrane tension and membrane-bending proteins organizes cell polarity during leading edge formation. *Nat Cell Biol* **17**, 749-758 (2015).

17. Douguet, D. & Honore, E. Mammalian mechanoelectrical transduction: structure and function of force-gated ion channels. *Cell* **179**, 340-354 (2019).

18. Shi, Z., Innes-Gold, S. & Cohen, A.E. Membrane tension propagation couples axon growth and collateral branching. *Sci Adv* **8**, eabo1297 (2022).

19. Gnanasambandam, R. *et al.* GsMTx4: Mechanism of Inhibiting Mechanosensitive Ion Channels. *Biophys J* **112**, 31-45 (2017).

20. Horigane, S.I., Ozawa, Y., Yamada, H. & Takemoto-Kimura, S. Calcium signalling: a key regulator of neuronal migration. *J Biochem* **165**, 401-409 (2019).

21. Valiente, M. & Marin, O. Neuronal migration mechanisms in development and disease. *Curr Opin Neurobiol* **20**, 68-78 (2010).

22. Stouffer, M.A., Golden, J.A. & Francis, F. Neuronal migration disorders: Focus on the cytoskeleton and epilepsy. *Neurobiol Dis* **92**, 18-45 (2016).

23. Baba, K. *et al.* Gradient-reading and mechano-effector machinery for netrin-1-induced axon guidance. *Elife* **7**, e34593 (2018).

24. Diz-Munoz, A., Fletcher, D.A. & Weiner, O.D. Use the force: membrane tension as an organizer of cell shape and motility. *Trends Cell Biol* **23**, 47-53 (2013).

25. Takahashi, Y. *et al.* High-speed SICM for the visualization of nanoscale dynamic structural changes in hippocampal neurons. *Anal Chem* **92**, 2159-2167 (2020).

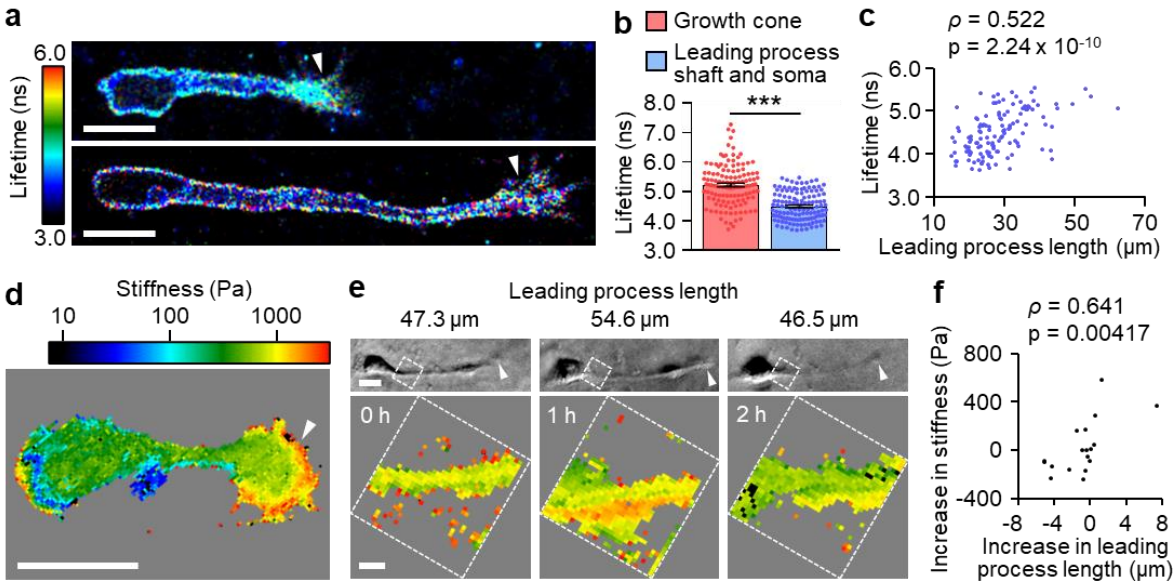

Fig. 1 | Leading process extension increases plasma membrane tension. a, Fluorescence lifetime images of Flipper-TR in olfactory interneurons with leading processes of different lengths. The colour bar indicates the lifetime in nanoseconds (ns). **b**, Fluorescence lifetime of Flipper-TR measured in the growth cone or in the leading process shaft and soma. n = 129 cells. Two-tailed Wilcoxon signed-rank test. ***$p < 0.01$. **c**, Fluorescence lifetime of Flipper-TR in the leading process shaft and soma plotted against the leading process length. n = 129 cells. Two-tailed Spearman's correlation coefficient (ρ) was calculated to determine the relationship between the membrane tension and the leading process length. **d**, A stiffness map of an olfactory interneuron produced by SICM. **e**, Bright field images (upper) and stiffness maps (lower) of a migrating olfactory interneuron acquired at 1-h intervals. The arrowheads indicate the growth cone. The stiffness of the plasma membrane was measured at the proximal leading process indicated by the boxes. **f**, The increase in the stiffness plotted against the increase in the leading process length. The first measurements were set as 0 as controls and omitted from the plot. n = 27 measurements from 9 cells. Two-tailed Spearman's correlation coefficient (ρ) was calculated to determine the relationship between the stiffness and the leading process length. Scale bars, 10 μm (**a**, **d** and **e**, upper); 2 μm (**e**, lower).

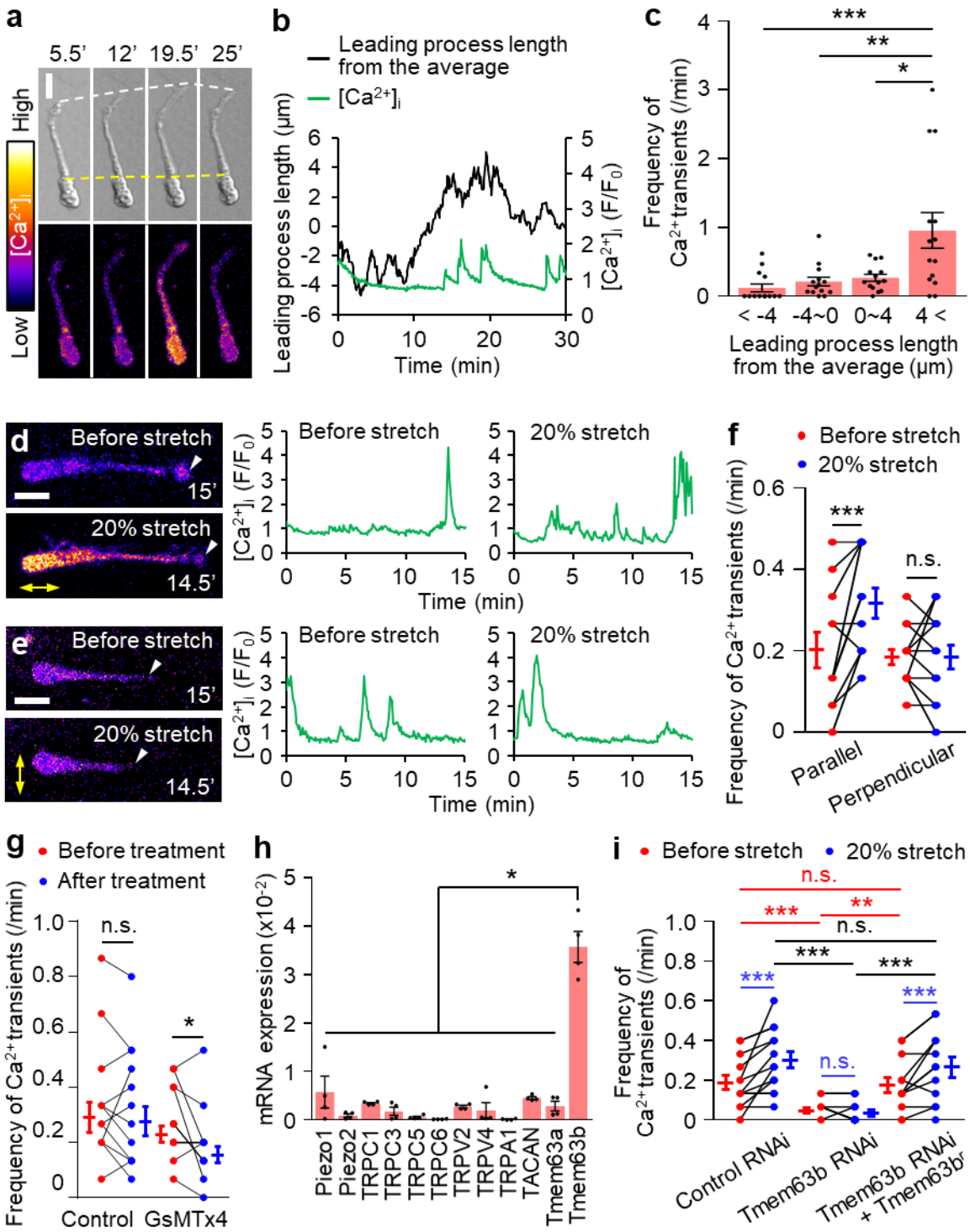

Fig. 2 | Leading process extension triggers Ca^{2+} transients via Tmem63b. a, Time-lapse DIC (upper) and $[Ca^{2+}]_i$ (lower) images of a migrating olfactory interneuron loaded with 1 μM CalRed R525/650. $[Ca^{2+}]_i$ is indicated as the ratio of the fluorescence intensity

at 525 nm to that at 650 nm. The white and yellow dashed lines indicate the fronts of the growth cone and soma, respectively. See Supplementary Video 1. **b**, Time course of the leading process length and $[Ca^{2+}]_i$ of the neuron shown in (**a)**. The average leading process length was set as 0. **c**, Relationship between the average leading process length and the frequency of Ca^{2+} transients. The frequency of Ca^{2+} transients was measured during increases and decreases in the neurite length. n = 56 measurements from 14 cells. **d** and **e**, Representative images of $[Ca^{2+}]_i$ of migrating olfactory interneurons (left) and the time courses of $[Ca^{2+}]_i$ (right). Neurons cultured on elastic chambers were imaged at 5-sec intervals for 15 min before (control) and after 20% stretch (yellow arrows). The arrowheads indicate the growth cones. We selected migrating olfactory interneurons with leading processes oriented parallel (**d**) or perpendicular (**e**) to the stretch direction. See Supplementary Video 3. **f**, The frequency of Ca^{2+} transients in migrating neurons before and after 20% stretch. Parallel, n = 11 cells; perpendicular, n = 12 cells. **g**, The frequency of Ca^{2+} transients in migrating olfactory interneurons before and after treatment with vehicle control (n = 12 cells) or 5 μM GsMTx4 (n = 13 cells). **h**, Expression of mechanosensitive ion channels in olfactory interneurons. The mRNA of the mechanosensitive ion channels was quantified with qPCR and normalized to the expression level of GAPDH. n = 4 independent experiments. **i**, Tmem63b knockdown abolishes the extension-triggered Ca^{2+} transient. The frequency of Ca^{2+} transients in migrating olfactory interneurons before and after 20% stretch. Control miRNA, n = 13 cells; Tmem63b miRNA, n = 12 cells; Tmem63b miRNA + RNAi-refractory Tmem63b ($Tmem63b^r$), n = 12 cells. Data represent mean ± SEM. Statistical analysis was performed using the two-tailed Mann–Whitney *U*-test (**c** and **h**), two-tailed paired *t*-test (**f** and **i**, blue), two-tailed Wilcoxon signed-rank test (**g**) and two-tailed one-way ANOVA with Tukey's post hoc test (**i**, red and black). *$p < 0.05$; **$p < 0.02$; ***$p < 0.01$; n.s., no significant difference. Scale bars, 10 μm (**a**, **d** and **e**).

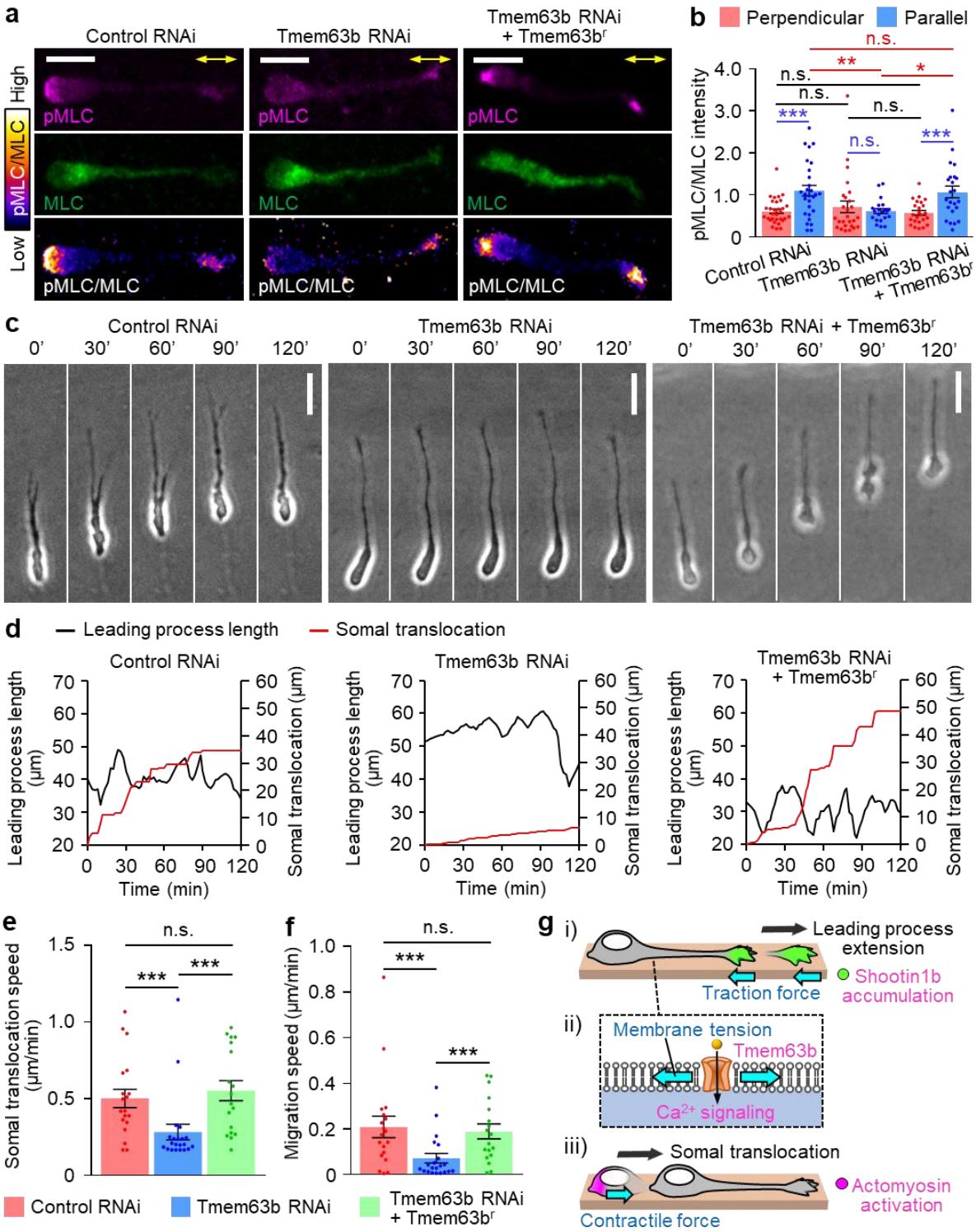

Fig. 3 | Tmem63b knockdown inhibits stretch-induced myosin II activation and somal translocation. a, Analyses of myosin II activity in olfactory interneurons expressing control miRNA, Tmem63b miRNA or Tmem63b miRNA + Tmem63b^r. Olfactory interneurons cultured on elastic chambers were fixed after 20% stretch, and

then stained with anti-phospho-myosin light chain 2 (pMLC) antibody (magenta), anti-myosin light chain 2 (MLC) antibody (green) and DAPI. The ratio of the fluorescence intensity of pMLC to that of MLC (pMLC/MLC) is displayed by the pseudocolour bar. Neurons with leading processes oriented parallel to the stretch direction (yellow arrows) were analysed. **b**, Statistical analysis of myosin II activity in olfactory interneurons from the data shown in (**a**). Myosin II activity (pMLC/MLC) was analysed at the rear of the cell soma (**Extended Data Fig. 5a**). Control RNAi: perpendicular, n = 31 cells; parallel, n = 28 cells. Tmem63b RNAi: perpendicular, n = 26 cells; parallel, n = 21 cells. Tmem63b RNAi + Tmem63b^{r}: perpendicular, n = 24 cells; parallel, n = 23 cells. **c**, Time-lapse images of migrating olfactory interneurons expressing control miRNA, Tmem63b miRNA or Tmem63b miRNA + Tmem63b^{r}. Images were acquired at 2-min intervals for 120 min. See Supplementary Video 4. **d,** Leading process length (black lines) and somal translocation (red lines) of olfactory interneurons shown in (**c**). **e** and **f**, Somal translocation speed (**d**) and migration speed (**e**) of olfactory interneurons shown in (**c**). Control miRNA, n = 19 cells; Tmem63b miRNA, n = 21 cells; Tmem63b miRNA + Tmem63b^{r}, n = 18 cells. **f**, A mechanical model of saltatory neuronal migration. i) Shootin1b accumulates at the leading process growth cone (green) and couples F-actin retrograde flow and the extracellular substrate, thereby generating traction force to drive leading process extension (see **Extended Data Fig. 1a**). ii) The increase in the process length elevates the plasma membrane tension. The elevated membrane tension activates Tmem63b, which induces Ca^{2+} influx and triggers Ca^{2+} signalling. iii) Upon activation induced by Ca^{2+} signalling, actomyosin (magenta) produces contractile forces, pushing the nucleus forward and driving somal translocation. Data represent mean ± SEM. Statistical analysis was performed using the two-tailed Mann–Whitney *U*-test (**b**, blue) and two-tailed Kruskal–Wallis test with Dunn's post hoc test (**b**, red and black, **d** and **e**). *$p < 0.05$; **$p < 0.02$; ***$p < 0.01$; n.s., no significant difference. Scale bars, 10 μm.